Cenomanian-Turonian sea-level transgression and OAE2 deposition in the Western Narmada Basin, India

Gerta Keller [a,*], Madan L. Nagori [b], Maya Chaudhary [b], A. Nallapa Reddy [c], B.C. Jaiprakash [d], Jorge E. Spangenberg [e], Paula Mateo [f], Thierry Adatte [g]

[a] Department of Geosciences, Princeton University, Princeton, NJ 08544, USA
[b] Department of Geology, Mohanlal Sukhadia University, Udaipur, Rajasthan, India
[c] Majestic Shore, 208 Choolaimedu High Road, Chennai 600094, India.
[d] Anagha, 4th Cross Street, CB Nagar, Tumkur 572102, India.
[e] Institute of Earth Surface Dynamics (IDYST), University of Lausanne, Lausanne 1015, Switzerland
[f] Division of Geological and Planetary Sciences, California Institute of Technology, Pasadena, CA 91125, USA
[g] Institute of Earth Sciences, University of Lausanne, Lausanne 1015, Switzerland

ARTICLE INFO

ABSTRACT

We report the Narmada Seaway began in India during the largest global sea-level transgression and Oceanic Anoxic Event 2 (OAE2) $\delta^{13}C$ excursion during the late Cenomanian to early Turonian. The transgression progressed eastward during the Turonian-Coniacian and reached Jhilmili by the end of the Maastrichtian. During this time the Narmada and Godavari Seaways may have joined via the Narmada-Tapti rift and formed a Trans-India Seaway. The history of this major seaway is entombed in a fossil-rich marine transgression of the tectonically active Narmada rift zone. We examined this transgression in the western Narmada Basin, Gujarat, to improve age control based on planktic foraminifera and ostracods and evaluate paleoenvironmental changes based on the Cenomanian-Turonian OAE2 $\delta^{13}C$ excursion, $\delta^{18}O$ records, and mercury concentrations in sediments as index for volcanic eruptions.

Results reveal the onset of the OAE2 $\delta^{13}C$ excursion began in the western Narmada Basin during the late Cenomanian coeval with the sea-level transgression and first influx of planktic and benthic foraminifera in the Nimar Sandstone that overlies Archean rocks. The OAE2 $\delta^{13}C$ excursion peak was recorded in oyster biostromes followed by fluctuating values of the $\delta^{13}C$ plateau in the overlying Limestone with oysters beds, and gradual decrease to background values by the early Turonian. We tested the age of the transgression and $\delta^{13}C$ excursion based on planktic foraminifera and ostracod biostratigraphy and successfully compared the results with the Pueblo, Colorado, Global Section and Stratotype Point (GSSP), and the eastern Sinai Wadi El Ghaib section of Egypt.

© 2021 International Association for Gondwana Research. Published by Elsevier B.V. All rights reserved.

1. Introduction

The Narmada Basin in India is an intracratonic rift basin of intense interest because of its tectonic history and northward journey after the breakup of Gondwana in the Early Cretaceous ~130 Ma (Tandon, 2000; Chatterjee et al., 2013; Kumari et al., 2020). Madagascar separated from India during the Turonian to Santonian transition and from the Seychelles during the Campanian to early Maastrichtian. Highlights of this journey are recorded in the Bagh Group exposed in disconnected outcrops along the edges of the Deccan basalt, and overlie Precambrian rocks from Madhya Pradesh to Gujarat (Tandon, 2000; Tripathi, 2006; Tripathi, 2005; Kumari et al., 2020) (Fig. 1).

Sediment deposition in the Narmada Basin occurred in a tectonic graben that was largely controlled by uplift, block faulting, volcanic activity, erosion and sea level transgressions (Biswas, 1987; Kumar et al., 1999; Tandon, 2000; Tripathi, 2006; Bansal et al., 2020; review in Kumari et al., 2020). Clues to this history can be found in the Late Cretaceous sediments roughly parallel to the present course of the Narmada River. In both eastern and western parts of the Narmada Basin, the Nimar Sandstone overlies the Archean crystalline basement rocks in a westerly sloping basin (Tripathi, 2006). However, the overlying sedimentary sequences vary.

In the eastern (upper) Narmada Basin of Madhya Pradesh, the fossiliferous marine transgression of the Bagh Group consists of Nodular Limestone, Chirakhan marl and Coralline Limestone topped by glauconite and overlain by the Maastrichtian Lameta Formation (Chiplonkar, 1982; Bansal et al., 2020). The eastern Bagh Group has been extensively

* Corresponding author.
  E-mail address: gkeller@princeton.edu (G. Keller).
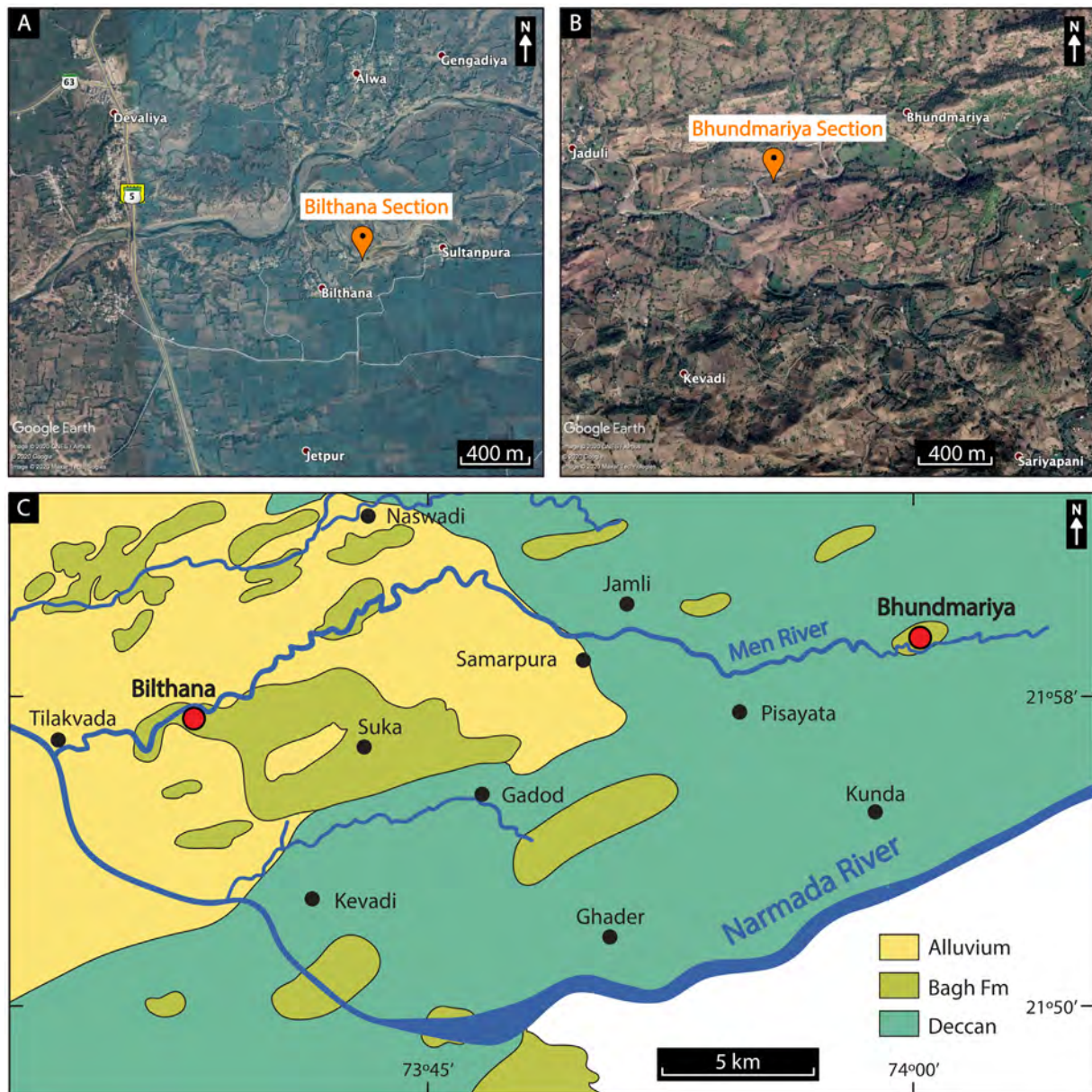
Fig. 1. (A) Google Earth image of the Bilthana study site, located near the village of Bilthana, along the Men River (N 21° 57′; E 73° 39′). (B) Google Earth image of the Bhundmariya study site, located near the village of Bhundmariya, along the Men River (N 21° 59′; E 73° 59′). (C) Geologic map of Bilthana and Bhundmariya study sites showing the location of Bagh Group outcrops.

studied based on ammonoids, ostracods, echinoids, bryozoan, marine algae and planktic foraminifera with ages attributed to the Turonian-Coniacian (Jain, 1975; Chiplonkar, 1982; Nayak, 1987; Chaudhary and Nagori, 2019). A recent study of ammonites and inoceramids in the Nodular Limestone revealed early, middle and late Turonian deposition (Kumar et al., 2018). These deposits mark the eastward-reach of a sea-level transgression during the Turonian (Tandon, 2000; Tripathi, 2006; Bansal et al., 2020; Kumari et al., 2020) and unconformably overlie the predominantly continental Nimar Sandstone.

In the western Narmada Basin of Gujarat, the Turonian-Coniacian limestone units of the Bagh Group from Madhya Pradesh are not present, likely because of tectonic activity, uplift, erosion and non-deposition (Tripathi, 2006). Instead, the estuarine facies of the Nimar Sandstone underlie in ascending order, a micritic sandstone, oyster beds and limestone with oysters, revealing the first major sea-level

transgression into the western Narmada Basin (Tandon, 2000; Tripathi, 2006). The depositional age was determined as Late Cenomanian to Early Turonian based on ostracods and calcareous algae (Kundal and Sanganwar, 1998; Chaudhary et al., 2017a).

The focus of this study is the first sea-level transgression into the western Narmada Basin in Gujarat during the late Cenomanian that originated central India's Narmada Seaway, which reached about 800 km across India by the end of the Maastrichtian (Keller et al., 2009). We explore whether this sea-level transgression could be linked to the global transgression that occurred during the late Cenomanian-early Turonian Oceanic Anoxic Event 2 (OAE2) based on two outcrops in Gujarat near the villages of Bilthana and Bhundmariya (Fig. 1A, B). We focus on four objectives: (1) improve biostratigraphy and age control; (2) determine the paleoenvironment and onset of the sea-level transgression; (3) identify the link between the sea-level transgression

and the OAE2; and (4) test the potential link between volcanism, LIPs, and Hg toxicity during this time.

Our investigations focus on biostratigraphy of planktic foraminifera and ostracods for age control, the nature of sediment deposition and characteristic fossil life for paleoenvironmental reconstructions, carbon isotopes for the identification of the OAE2, oxygen isotopes for paleoclimate and fresh water influx reconstructions, and mercury concentrations in sediments for assessing the potential influence (toxicity, warming) of large volcanic eruptions.

2. Materials and methods

We analyzed Bhundmariya and Bilthana localities from Gujarat in the western Narmada Basin. The Bilthana section is located near the village of Bilthana, along the Men River (N 21° 57′; E 73° 39′) (Fig. 1A, C). The Bhundmariya section, is located near the village of Bhundmariya, also along the Men River (N 21° 59′; E 73° 59′) (Fig. 1B, C). In both sections, the Nimar Sandstone followed by the Micritic Sandstone mark the base of the Bagh Group and disconformably overlie crystalline Archaean rocks. Above this interval, oyster biostromes transition into sandy Limestones with oysters at Bilthana and marly Limestone with oysters at Bhundmariya (Figs. 2, 3).

Samples were initially collected for ostracod biostratigraphy at 30, 60 and 100 cm intervals at Bilthana and analyzed for foraminifera, oxygen and carbon stable isotopes, and mercury concentrations. The Bhundmariya outcrop was collected at closer sample intervals (10–15 cm) to confirm the stratigraphic record and identify missing intervals.

For foraminifera biostratigraphy, samples were crushed into pea-sized fragments, placed in beakers and covered with a 3% hydrogen peroxide solution to oxidize organic carbon, and let stand for 24–48 h. After disaggregation of sediments, the sample residue was processed through >38 μm, >63 μm and > 150 μm screens to catch foraminifers in dwarfed, standard and larger size fractions, respectively. Cleaned residues were dried in the oven and analyzed for microfossils. Most lithologies are strongly micritized and foraminifera difficult to free from such sediments. Therefore, thin sections were also prepared for planktic foraminiferal analyses. Preservation is poor due to recrystallized foraminiferal shells in micritized sandstones and limestones. Species identifications are based on processed samples and thin sections. Identification of recrystallized specimens is mainly restricted to larger species with recognizable number of chambers, shape and keel characteristics.

The concentration of mercury in the sediment was analyzed at the Geosciences Department of Princeton University (USA) using a Zeeman R-915F (Lumex, St. Petersburg, Russia), a high-frequency atomic absorption spectrometer specifically designed for Hg determination with a detection limit of 0.3–3 ppb. Measurements are based on the direct thermal evaporation of Hg from solid samples and do not require chemical pre-treatment of samples, thus avoiding potential contamination during sample preparation. Analyses were conducted on two aliquots. Accuracy of the measurements was confirmed by the analysis of certified reference materials NIST 1646a with Hg calibrated at 30.2 ppb.
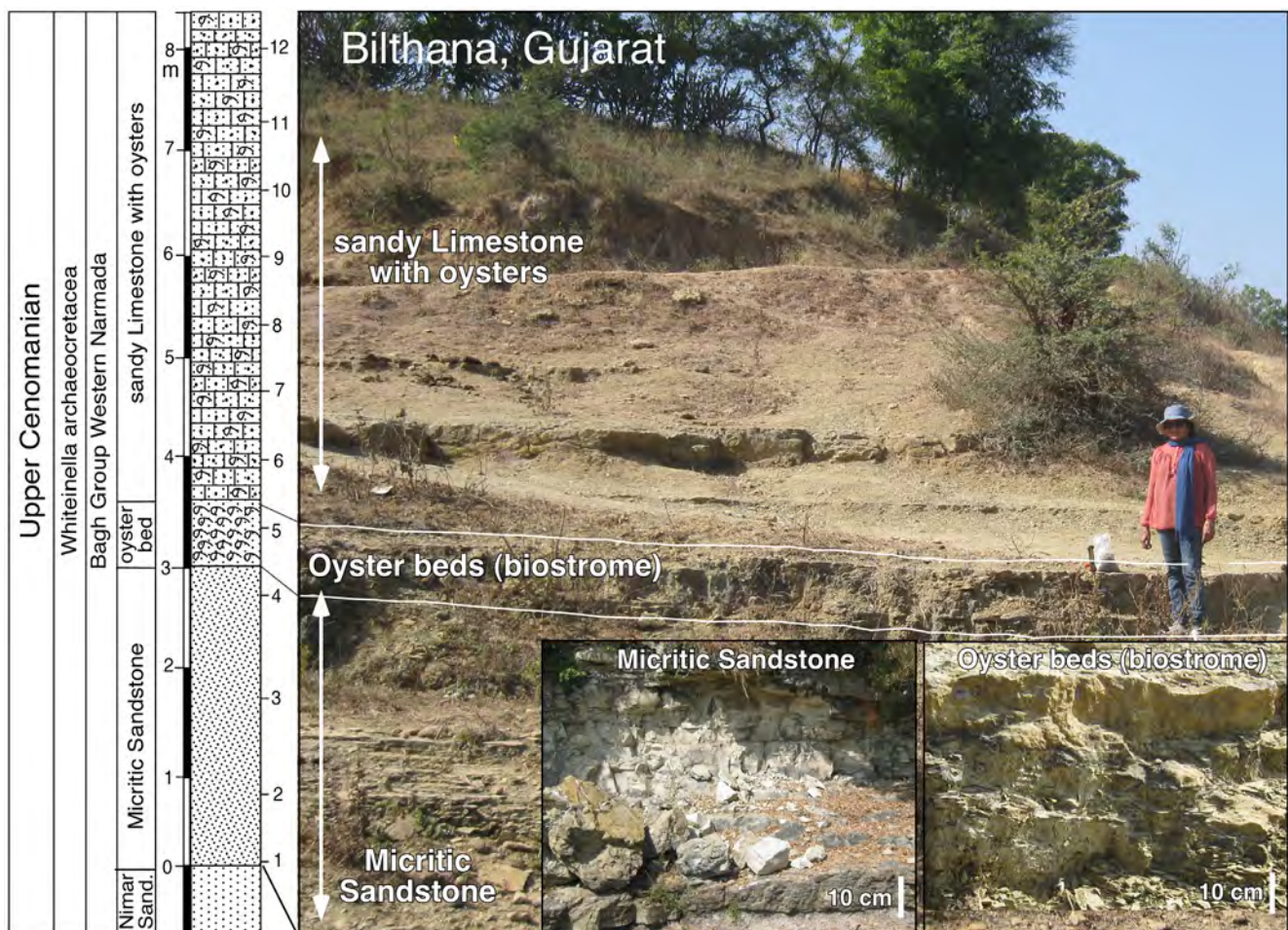
Fig. 2. Panorama view of the Bilthana outcrop (Gujarat), which consist of the Nimar Sandstone and overlying Micritic Sandstone at the base, followed by oyster beds that transition into sandy Limestones with oysters at Bilthana. Inserts show close-up views of bedded micritic sandstone and oyster beds.

Fig. 3. Panorama view of the Bhundmariya outcrop (Gujarat) with Nimar Sandstone and Micritic Sandstone at the base followed by a thin oyster bed and thick unit of marly Limestone with oysters. Note the first 10 m of this outcrop were analyzed with the top 10 m just below the white sample bag to the left of the photo.

Precision based on relative standard deviation of repeated sample measurements is 5–10%.

Total organic carbon (TOC) contents were determined at the Institute of Earth Sciences, University of Lausanne (Switzerland) based on RockEval™ 6 and quantified by flame-ionization and infrared detection. The IFP 160000 Rock-Eval standard was used for calibration. Analytical precision is 0.05 wt%. Results show TOC consistently <0.02 wt% likely due to diagenetic alteration of organic matter as evident by tan orange and ochre outcrop colors.

Carbon and oxygen stable isotope analyses were performed on bulk rock sediments at the Institute of Earth Surface Dynamics (ISTE) of the University of Lausanne (Switzerland) using a Thermo Fisher GasBench II preparation device interfaced with a Thermo Fisher Delta Plus XL continuous flow isotope ratio mass spectrometer. The carbon and oxygen stable isotope ratios are reported in the delta (δ) notation as the permil (‰) deviation relative to the Vienna Pee Dee belemnite standard (VPDB). The reproducibility was better than 0.05‰ for $\delta^{13}C$ and 0.1‰ for $\delta^{18}O$.

3. Age and biostratigraphy

The Nimar and Micritic Sandstones are the oldest sediments overlying the Archean crystalline rocks in this area and the age was previously attributed to the Cenomanian based on ostracods and calcareous algae (Kundal and Sanganwar, 1998; Chaudhary et al., 2019). Planktic foraminifera are rare to few, small, long-ranging and stress tolerant species but not age diagnostic (*Muricohedbergella, Planoheterohelix, Heterohelix*). Benthic foraminifera are generally long-ranging and not useful age indicators either (*Haplophragmoides, Textularia, Spiroplectammina, Trochammina, Dentalina, Vaginulina*) (Rajshekhar, 1987, 1995; Rajshekhar and Atpalkar, 1995). A summary of previous biostratigraphic studies based on a large variety of fossils (e.g., ammonites,

inoceramids, ostracods, echinoids, benthic and planktic foraminifera, calcareous algae) in the Bagh Group of the western Narmada Basin is shown in Table 1 (references therein).

In the Limestones with oysters overlying the Nimar and Micritic Sandstones, ostracods are common to abundant at Bilthana and Bhundmariya during the late Cenomanian, as identified by the index species *Rostrocytheridea divergens, R. jaisalmerensis* and *Cytherella okadai*. These species are present in the Micritic Sandstone, as well as the overlying oyster beds and Limestone with oysters (Chaudhary et al., 2017a, 2017b, 2019; Chaudhary and Nagori, 2019) (Figs. 4, 5). Previously, the undifferentiated Cenomanian age was assigned (Jain, 1961; Chiplonkar, 1982; Nayak, 1987; Rajshekhar, 1987, 1995; Rajshekhar and Atpalkar, 1995).

Planktic foraminifera at Bilthana and Bhundmariya localities are common to abundant in the oyster beds and Limestone with oysters, but benthic foraminifera are rare or absent. A single low salinity tolerant planktic foraminifer, *Muricohedbergella delrioensis*, thrived in the oyster biostrome and oyster-rich sandy Limestone at Bilthana. Also present are rare *Whiteinella archaeocretacea* (Plate 1), the index species that marks the latest Cenomanian to early Turonian *W. archaeocretacea* zone, which coincides with the OAE2 (Leckie, 1987; Leckie et al., 1998; Keller et al., 2001, 2004, 2008; Keller and Pardo, 2004; Gertsch et al., 2008, 2010; Heimhofer et al., 2018). Benthic foraminifera include the brackish water tolerant *Anomalinoides newmanae* and diverse arenaceous species (Fig. 4).

At Bhundmariya, more diverse planktic foraminiferal assemblages survived in the marly Limestone with oysters. In the basal 1.5 m of the section, *M. delrioensis* dominated with few *Muricohedbergella hoelzli* and *Muricohedbergella simplex* species (Figs. 3, 5). Diversity increased with the appearance of larger species, including *W. archaeocretacea, Whiteinella baltica, Whiteinella brittonensis, Dicarinella imbricata* and *Dicarinella hagni,* providing good biostratigraphic age control during the late Cenomanian-early Turonian OAE2.

Table 1

Summary of fossil contents and age diagnostic species (bold) of ostracods, ammonites and planktic foraminifera in late Cenomanian sediments. This is the first application of shallow, near-shore planktic foraminiferal assemblages to identify the OAE2 in the western India interior seaway of the Narmada Valley, although such applications have been successfully done in Egypt and Morocco (Keller et al., 2008; Gertsch et al., 2008, 2010; El-Sabbagh et al., 2011).

Stage, Age (Ma)	Group	Formation/Members	Ammonites, Inoceramids, Other	Ostracods	Planktic Foraminifera	References
Early Turonian, 90	Bagh	Limstone with oysters	Chiplonkarina dimorphopora Placenticeras mintoi	Amicytheridea bilthanensis **Rostrocytheridea jaisalmerensis** **Rostrocytheridea divergens**	Whiteinella baltica **W. archaeocretacea** W. brittonensis	*Ammonites and Inoceramids:* Gangopadhyay and Bardhan 2007; Jaitley and Ajane 2013
Late Cenomanian OAE2, 94		Oyster beds and biostromes		Haughtonileberis thuatiensis Paracypris jaini	**Dicarinella hagni** **Dicarinella imbricata**	*Calcareous algae:* Kundal and Sanganwar 1998
				Sapucariella cf subtriangulata **Cytherella okadai**	Muricohedbergella delrioensis, H. hoelzli	*Ostracods:* This study; Jain 1975; Singh 1997; Chaudhary et al 2017a,b; Chaudhary and Nagori, 2019; Chaudhary et al 2019
Early Late Cenomanian, 96-6-96.4		Micritic Sandstone		Paijenborchella jeerabadensis	H. simplex	
			Calcareous algae	**Rostrocytheridea jaisalmerensis**	Planoheterohelix*	*Foraminifera:* This study; Rajshekhar 1987, 1995*; Nayak, 1987; Leckie et al., 1987, 1998; Rajshekhar and Atpalkar 1995*; Keller and Pardo 2004; Keller et al 2004, 2008
		Nimar Sandstone		**Rostrocytheridea divergens**	Heterohelix* Muricohedbergella*	
Archean, 2500		Crystalline rocks				

3.1. Late Cenomanian-early Turonian OAE2

The late Cenomanian to early Turonian is an extremely well-studied interval because the global OAE2 occurred during this transition. Age-defining biozones characteristic of OAE2 are commonly based on ammonites, inoceramids, and deep-sea planktic foraminifera. We illustrate these biozonations along with the defining OAE2 δ^{13}C excursion based on the Global Stratotype Section and Point (GSSP) in Pueblo, Colorado (USA), where sediment deposition occurred in the middle neritic environment of the USA Western Interior Seaway (Leckie, 1987; Leckie
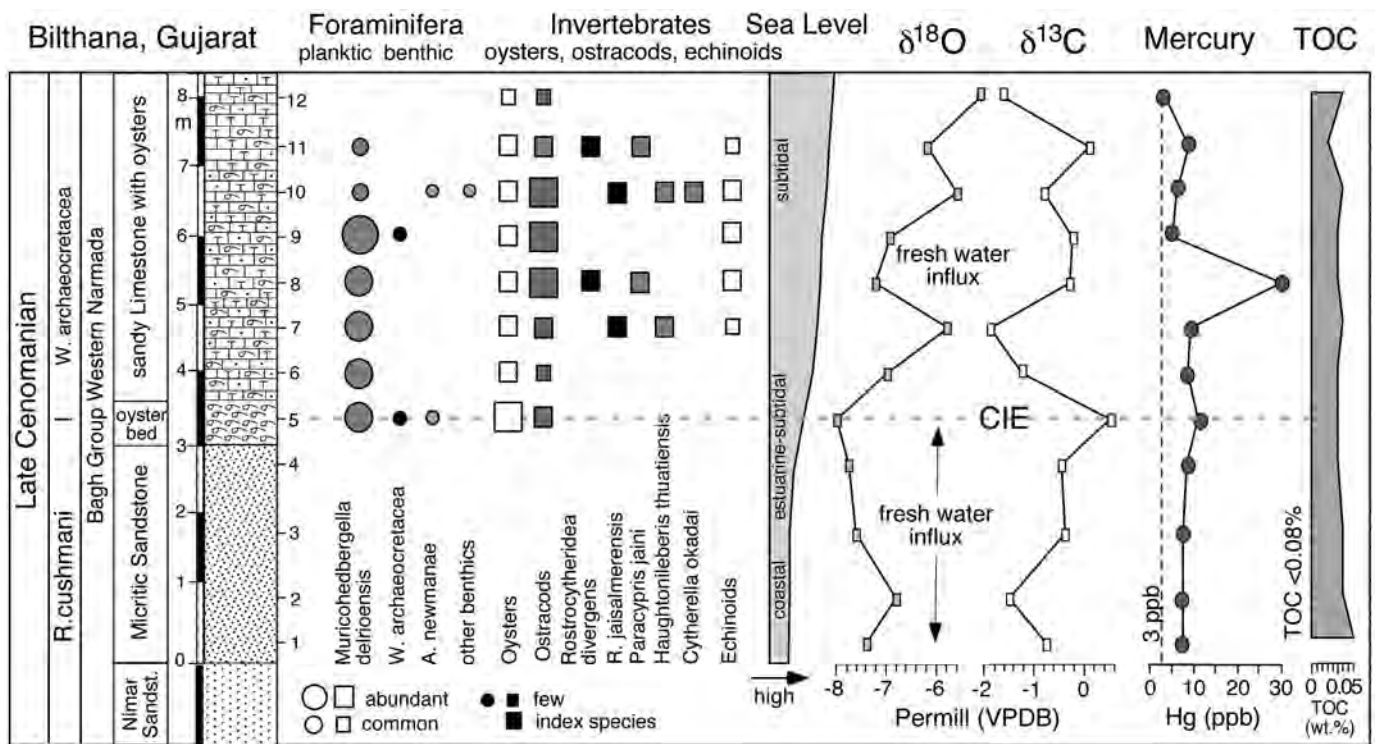
Fig. 4. Late Cenomanian biostratigraphy, faunal and environmental changes at Bilthana, Gujarat. Low diversity but abundant small planktic and rare benthic foraminifera, common to abundant oysters, ostracods and echinoids are indicative of shallow, near-shore environments. Near absence of benthic foraminifera is likely due to the brackish water environment. Oyster biostromes mark the sea-level transgression. δ^{18}O data are compromised by diagenesis and salinity effects. The mercury anomaly suggests volcanic eruptions during the late Cenomanian.
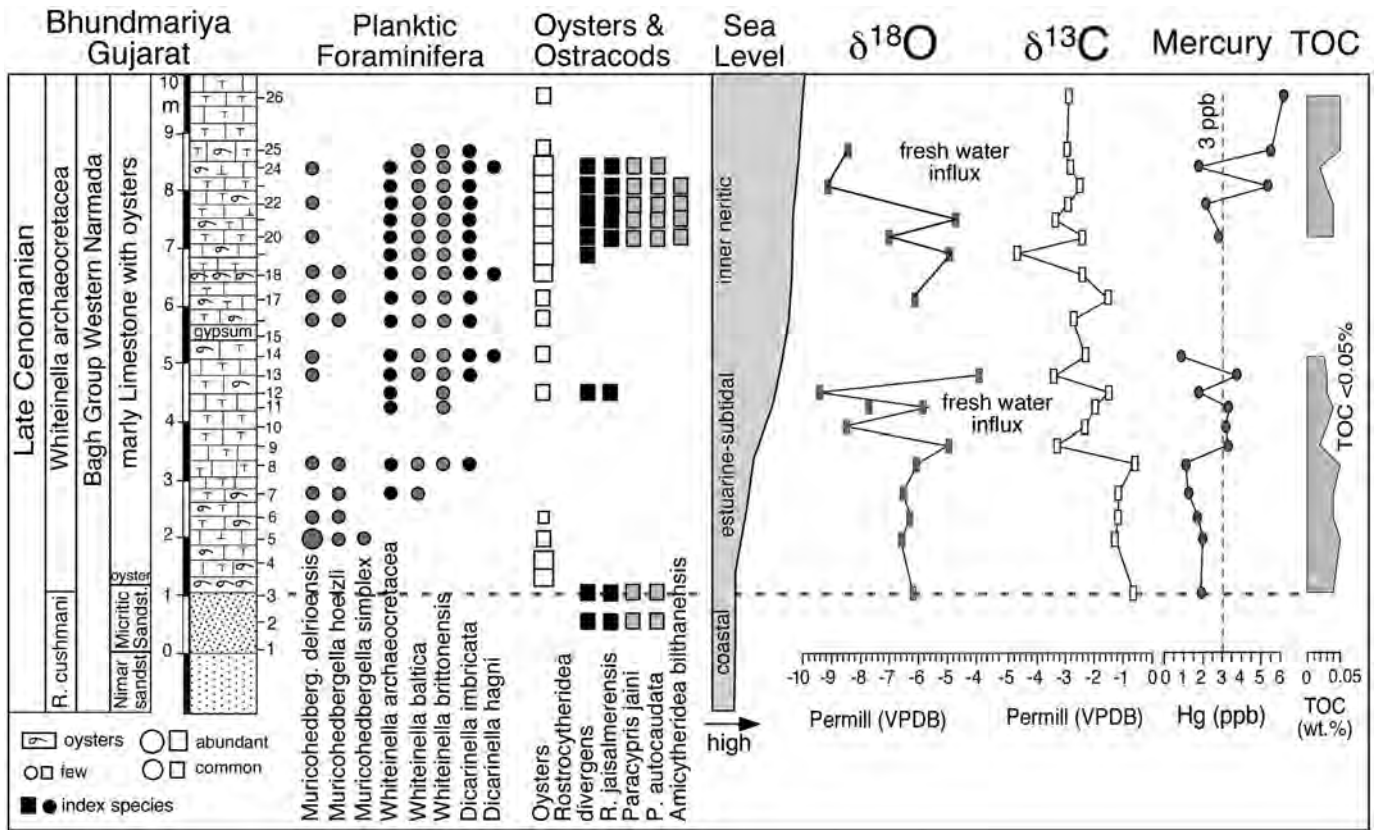
Fig. 5. Late Cenomanian biostratigraphy, faunal and environmental changes at Bhundmariya, Gujarat. Increased diversity of planktic foraminifera indicates slightly deeper subtidal water. Decreased diversity or absence of fauna correlates with the very negative δ18O excursions indicative of fresh water influx. Mercury concentrations are low and the record incomplete. The sea-level transgression is marked by oyster beds.

et al., 1998; Keller and Pardo, 2004; Keller et al., 2004; Caron et al., 2006) (Fig. 6). For age comparison with shallower environments, we plot the zonal schemes and OAE2 δ13C excursions of the subtidal to estuarine Wadi El Ghaib section in the eastern Sinai of Egypt (Gertsch et al., 2008) and the Gujarat sections of India (Fig. 6).

In the middle neritic environment of Pueblo and the estuarine to subtidal environment of the Sinai, ammonites have been commonly used for regional age control as shown for comparison with planktic foraminifera (Fig. 6). In the western Narmada Basin of Gujarat, only the monospecific nektobenthic ammonite *Placenticeras mintoi* was reported in the Nimar Sandstone (Gangopadhyay and Bardhan, 2007; Jaitley and Ajane, 2013). However, by Turonian age, the sea-level transgression reached middle neritic depths in the eastern Narmada Basin of Madhya Pradesh supporting diverse ammonites in the Nodular Limestones (Gangopadhyay and Bardhan, 2007; Kumar et al., 2018).

Planktic foraminifera are the most commonly used age-defining biozones characteristic of OAE2. The upper *Rotalipora cushmani* zone marks the gradual onset to the first peak of the OAE2 δ13C excursion, which coincides with the extinction of *R. cushmani*, the last survivor of this genus (Fig. 6). The *W. archaeocretacea* zone defines the interval from the *R. cushmani* extinction to the first appearance of *Helvetoglobotruncana helvetica* in the early Turonian. This interval spans most of the OAE2 δ13C excursion.

The *W. archaeocretacea* zone is subdivided into three subzones (Keller et al., 2004; Keller and Pardo, 2004), two of which span the Plenus Cold Event and maximum δ13C excursion (Fig. 6) (Keller and Pardo, 2004; O'Connor et al., 2020). Subzone *Globigerinelloides bentonensis* defines the interval between the *R. cushmani* extinction at the base and the *G. bentonensis* extinction at the top, but also coincides with the first appearances (FAs) of *D. imbricata* at the base and *D. hagni*

at the top. Subzone *D. hagni* defines the interval from the FA of this species to the *Planoheterohelix* shift, an interval dominated by low oxygen tolerant biserial species that continues into the early Turonian and ends with the return to normal δ13C values (Leckie, 1987; Leckie et al., 1998; Keller and Pardo, 2004; Keller et al., 2004).

Presence of the global OAE2 δ13C excursion in the open ocean and shallow near-shore sequences is an excellent correlation tool, provided sedimentation is relatively complete. The δ13C excursion began with a gradual rise to the maximum excursion coupled with the short Plenus cold event, also identified as the Plenus Carbon Isotope Excursion (CIE) (O'Connor et al., 2020). This event merged into a broad fluctuating δ13C plateau, followed by the gradual decrease to normal δ13C values in the early Turonian (Gertsch et al., 2008, 2010; Jarvis et al., 2011; O'Connor et al., 2020).

In the subtidal to estuarine environment of the Wadi El Ghaib in the Sinai, the OAE2 δ13C excursion is very similar to Pueblo, Colorado (Fig. 6). However, at Bilthana and Bhundmariya in the western Narmada Basin, the δ13C excursion peak is not well expressed due to incomplete sedimentation, erosion, non-deposition and partly low sample resolution. At Bilthana, sediment deposition occurred in a brackish estuarine environment dominated by the nearly monospecific assemblage of *M. delrioensis* but the OAE2 δ13C excursion peak is present in the oyster biostrome (Figs. 4, 6).

In contrast, the Bhundmariya section, just ~25 km from Bilthana, lacks oyster beds or oyster biostromes at the base of the Limestone with oysters and the OAE2 δ13C excursion peak is not observed (Figs. 5, 6). This suggests non-deposition or erosion (hiatus) of this interval, as also implied by the significantly deeper and more diverse, larger planktic foraminiferal assemblages, including late Cenomanian index species *D. imbricata* and *D. hagni*, beginning just 2 m above the
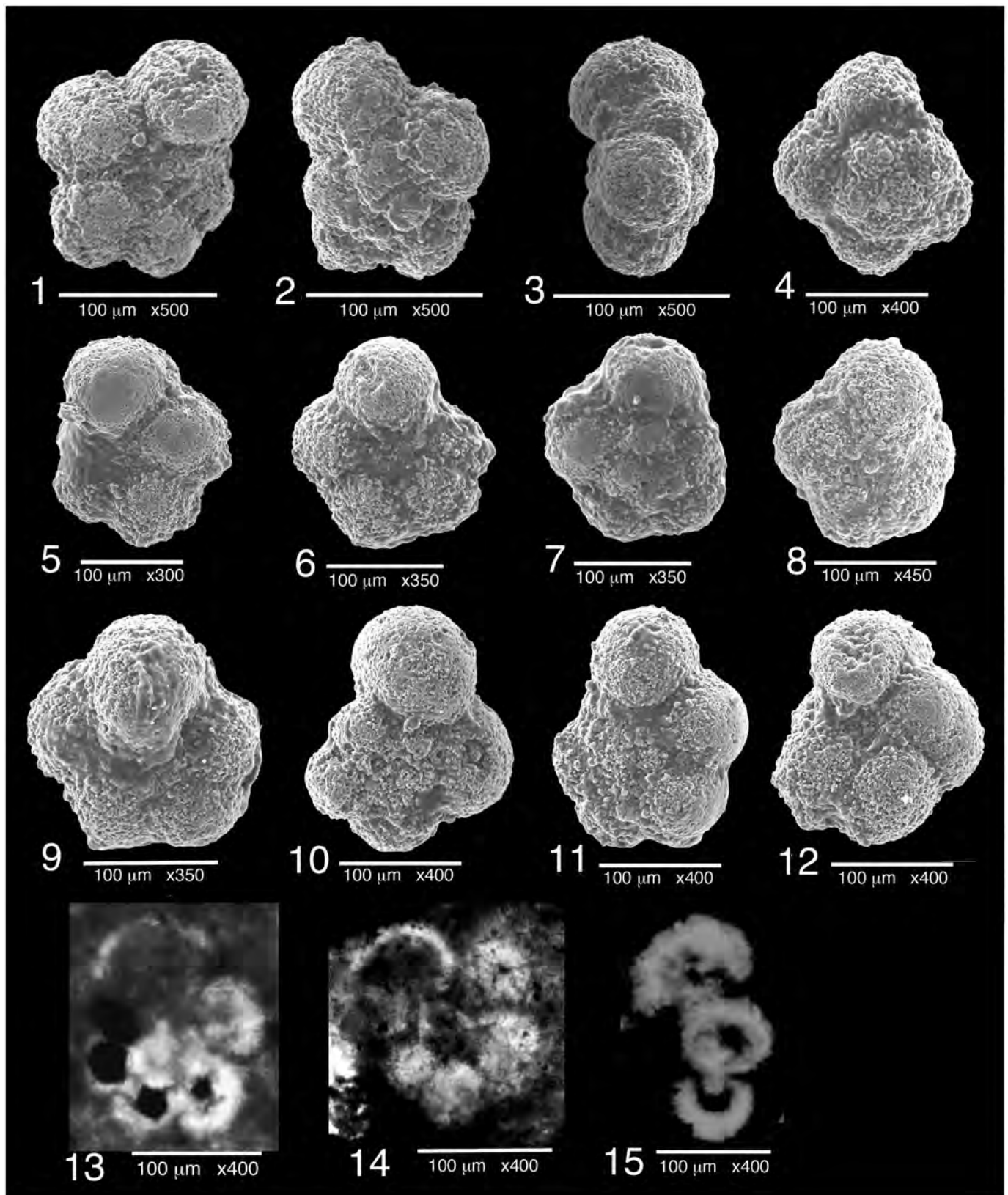
Plate 1. Common planktic foraminifera from the oyster beds and Limestone with oysters at Bilthana and Bhundmariya. Scale bar = 100 μm. Fig. 1–9 *Muricohedbergella delrioensis*, common to abundant small species tolerant of brackish water environments. Figs. 10–12. *Whiteinella archaeocretacea*, index species for late Cenomanian age and OAE2. Figs. 13–15. Thin section images of *Whiteinella archaeocretacea*, Bhundmariya. Similar *Muricohedbergella*-dominated assemblages have been documented in near-shore environments of Egypt, Morocco and USA (Pueblo, Colorado, GSSP) (Keller et al., 2004, 2008; Gertsch et al., 2008; El-Sabbagh et al., 2011).
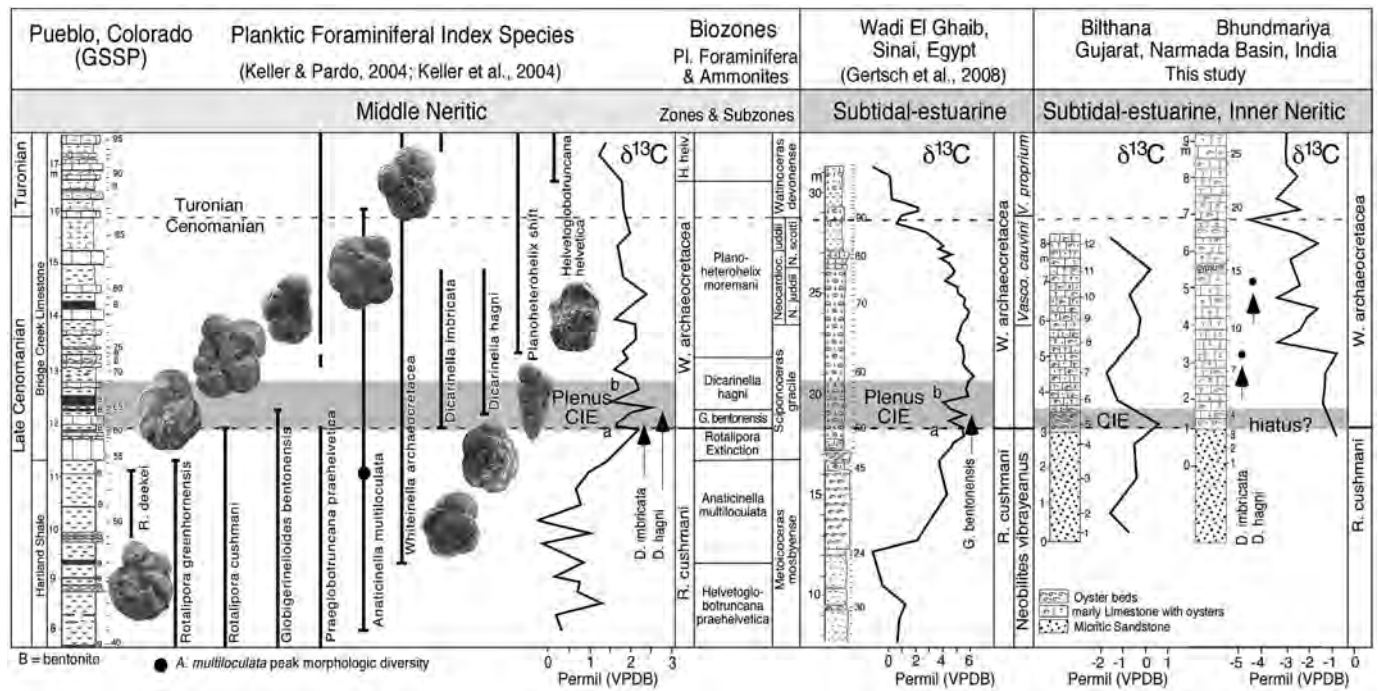
Fig. 6. Late Cenomanian biostratigraphy of planktic foraminifera and ammonites, and δ¹³C excursion characteristic of the OAE2 at the GSSP at Pueblo, Colorado (USA) (Keller and Pardo, 2004; Keller et al., 2004), compared and correlated with subtidal-estuarine sections from the Sinai (Egypt; Gertsch et al., 2008) and Gujarat (India). Note the onset of the global δ¹³C excursion is present in Gujarat with the overall OAE2 δ¹³C trend preserved in an environment alternating between brackish and normal marine salinities.

Micritic Sandstone (Fig. 5). These index species are absent at Bilthana's shallower estuarine environment dominated by the salinity tolerant *M. delrioensis*. Nevertheless, the mere presence of these index species, which evolved during OAE2 after the δ¹³C excursion peak reflects the OAE2 plateau correlative with Pueblo, Colorado, and the Wadi El Ghaib Sinai sections (Fig. 6). We conclude, the biostratigraphic correlation between the western Narmada Basin with sections at Pueblo, Colorado and the Sinai based on planktic foraminifera index species provides good age control and reveals the presence of OAE2 in all three localities.

3.2. Paleoenvironment

Few planktic foraminiferal species survive in high-stress, shallow neritic environments, such as the western Narmada Basin during the late Cenomanian to early Turonian. Survivor species are generally tolerant of variations in oxygen, salinity, temperature, nutrients and toxicity (e.g., mercury from large volcanic eruptions) (Keller, 2003; Keller et al., 2007, Keller et al., 2020). These species tend to be small, unornamented with simple test morphologies (biserial, triserial, trochospiral) and frequently dwarfed in high-stress environments (Leckie et al., 1998; Keller and Abramovich, 2009). Depending on the degree of biotic stress, foraminiferal assemblages vary from few species in shallow neritic environments to a single survivor in brackish estuarine conditions. During the late Cenomanian OAE2, one to six survivor species was the norm in shallow neritic environments of the Tethys from Egypt to Morocco and the USA Western Interior Seaway (Leckie, 1987; Leckie et al., 1998; Keller and Pardo, 2004; Keller et al., 2004; Gertsch et al., 2008, 2010; El-Sabbagh et al., 2011).

In the Nimar and Micritic Sandstones of the Gujarat sections, few small planktic foraminifera from *Planoheterohelix* and *Heterohelix* genera were reported along with arenaceous benthic foraminifers (*Haplophragmoides, Textularia, Spiroplectammina, Trochammina, Dentalina, Vaginulina*) (Rajshekhar, 1987, 1995; Rajshekhar and Atpalkar, 1995). These benthic species indicate deposition in an estuarine environment, consistent with the onset of the first sea-level transgression into the Narmada Basin. However, heterohelicid species

(e.g., *Heterohelix globulosa, Planoheterohelix moremani*) generally thrived in the oxygen minimum zone of deeper neritic environments (Leckie, 1987; Leckie et al., 1998; Keller and Pardo, 2004) and may have washed into this estuarine environment, as suggested by their absence in the rest of the sequence.

At Bilthana, the oyster biostromes above the Nimar and Micritic Sandstones, are characteristic of high-energy, shallow and faunally restricted environments with low salinity and mesotrophic nutrient levels (Pufahl and James, 2006). Deposition generally occurred in shallow subtidal (<20 m) and estuarine environments (Pufahl and James, 2006). With the deepening environment, the oyster biostrome morphed into a sandy Limestone with oysters and a nearly monospecific planktic foraminiferal assemblage thrived consisting of the low salinity tolerant *M. delrioensis* (Fig. 4, Plate 1). This species is tolerant of brackish waters, similar to *M. planispira* (Keller and Pardo, 2004). Benthic foraminifera are rare, including the low salinity tolerant brackish water *Anomalinoides newmanae*, and arenaceous species. Oysters, echinoids and ostracods are common. Towards the top of the sequence, the sharply decreased abundances of *M. delrioensis*, oysters, ostracods and echinoids may be related to deepening of the subtidal environment as the sea-level transgression progressed. These faunal changes occurred during the late Cenomanian *W. archaeocretacea* zone, as indicated by rare occurrences of this index species and also two ostracod index species, *Rostrocytheridea divergence* and *Rostrocytheridea jaisalmerensis* (Fig. 4). The overall high-stress environment and near absence of benthic foraminifera may also be amplified by relatively high mercury concentrations (8-9 ppb) and a one peak eruption event of 30 ppb. The high background Hg values suggest increased Hg runoff from land during the humid conditions resulting in toxicity for marine life (Grasby et al., 2020).

Bhundmariya reveals the biotic trend during the late Cenomanian *W. archaeocretacea* zone in the marly Limestone with oysters where the *Muricohedbergella* assemblage was followed by *Whiteinella* species but near absence of benthic foraminifera. The temporary disappearance of this assemblage (samples 9, 10; Fig. 5), coupled with negative δ¹⁸O (−3.4‰) and δ¹³C (−2.4‰) excursions and extreme δ¹⁸O data

fluctuations (−5‰ to −8.5‰), suggests fresh water influx and eutrophication. Above this barren interval, planktic foraminifera and ostracods are more diverse and species are larger and more complex (*Whiteinella* and *Dicarinella)*, which suggests migration of open marine planktic foraminifera into the deepening Narmada Seaway and thriving in more normal salinity and oxygen conditions and gradually decreasing δ^{13}C values. Near the top of the section, another fresh water event resulted in the negative (−4.5 to −9‰) δ^{18}O excursion indicative of fresh water influx and eliminating all but a few fossils. Mercury concentrations doubled, suggesting increased volcanic eruptions and/or mercury runoff from land during the humid conditions resulting in toxicity for marine life (Grasby et al., 2020).

4. Carbon and oxygen stable isotopes

We analyze carbon and oxygen stable isotopes of the Bhundmariya and Bilthana sections from Gujarat (Figs. 4, 5) to evaluate nutrient and salinity trends in shallow neritic environments during the OAE2. We compare the Gujarat δ^{13}C record with similar shallow marine sequences in the Tethys Ocean from the Sinai, Egypt, to Morocco and Pueblo, Colorado, USA Western Interior Seaway (Fig. 6). The OAE2 has a 2‰ to 3‰ positive δ^{13}C excursion, prolonged plateau and gradual decrease across the Cenomanian-Turonian boundary in shallow marine environments (Keller et al., 2004; Gertsch et al., 2008, 2010; El-Sabbagh et al., 2011; Jarvis et al., 2011; Bomou et al., 2013; Wendler, 2013; Kuhnt et al., 2017). Shallow neritic environments reveal this characteristic δ^{13}C excursion dependent on the continuity of the sedimentation record (Gertsch et al., 2008, 2010; O'Connor et al., 2020). We illustrate the OAE2 δ^{13}C excursion for Pueblo, Colorado, and the Sinai Wadi El Ghaib sections compared with the western Narmada Basin of India (Fig. 6).

The carbonate δ^{13}C values are generally not affected by diagenesis (Schrag et al., 1995), except for organic-rich sediments due to the diagenetic alteration of organic carbon (Pratt, 1984; Marshall, 1992). Cross-plots of δ^{13}C and δ^{18}O of the Sinai and Morocco sections revealed no significant correlation, thus indicating no major diagenetic alteration (Gertsch et al., 2008, 2010). In contrast, the Bilthana and Bhundmariya δ^{13}C records show intervals of significantly negative δ^{13}C values, which can only be explained by ^{13}C-depleted dissolved inorganic carbon (DIC) by contribution of oxidized organic carbon. The oxidation of organic matter is evident by the low TOC values and the tan-orange and ochre colors of the sediments. This early diagenetic alteration of more abundant organic matter in well-oxygenated shallow to middle neritic environments may have produced ^{13}C depleted CO_2 that contributed to the DIC involved during neoformation/recrystallization of the carbonate phases.

Bilthana and Bhundmariya sections mark overlapping parts of the OAE2 δ^{13}C excursion with the major difference in the variable sedimentation/erosion patterns and the lower sample resolution (Fig. 6). The overall more positive δ^{13}C ratios at Bilthana can be explained by higher terrestrial influx nearer to shore, which is also evident in the sandy limestone. More negative δ^{13}C ratios at Bhundmariya reflect early diagenetic alteration of abundant organic matter in well-oxygenated shallow to middle neritic environments (discussed above). These two δ^{13}C records for Gujarat are successfully compared with the biostratigraphy of the Tethys Seaway (Morocco, Egypt) and the Western Interior Seaway (Pueblo, Colorado, USA) (Fig. 6).

4.1. δ^{18}O excursions: Fresh water influx

Diagenesis primarily affects oxygen isotope values and renders them unreliable for temperature trends (e.g., Schrag et al., 1995). Particularly, the effects of recrystallization and high capacity of oxygen exchange in interstitial fluids leads to negative δ^{18}O values (Gertsch et al., 2008). However, very negative δ^{18}O ratios yield evidence of fresh water influx (Ghosh et al., 1995). For example, well-preserved *Muricohedbergella planispira* at Pueblo, Colorado, measured δ^{18}O ratios from −12‰ to

−2‰ and yielded a record of cyclic variations of fresh water influx (Keller and Pardo, 2004; Keller et al., 2004). Similarly, negative δ^{18}O ratios (−9‰ to −3‰) were reported from shallow marine OAE2 sequences with oyster-rich limestones in the Sinai, Egypt, and Morocco, and mainly attributed to fresh water influx (Kuhnt et al., 2004; Tsikos et al., 2004; Keller et al., 2004, 2008; Gertsch et al., 2008, 2010; El-Sabbagh et al., 2011).

In the Micritic Sandstone at Bilthana, Gujarat, the negative δ^{18}O ratios (−8‰ to −6.8‰) indicate fresh water influx, correlative with the gradual 2‰ positive δ^{13}C excursion and sea-level transgression associated with the OAE2 (Fig. 4). No foraminifera or invertebrates were observed in this interval. The second fresh water pulse (δ^{18}O -7‰, samples 8–9) correlates with the OAE2 δ^{13}C plateau. At Bhundmariya, the correlative fresh water influx (δ^{18}O -9.5‰, samples 10–12) also marks the OAE2 δ^{13}C plateau (Fig. 5). In both localities, the fresh water influx resulted in absent or strongly reduced marine life, as also observed in the fresh water pulse near the top of the Bhundmariya section.

5. Mercury

Mercury anomalies in sediments worldwide have been identified as potential proxy for Large Igneous Province (LIP) volcanism associated with all five major mass extinctions in Earth's history (e.g., Grasby et al., 2016; Gong et al., 2017; Jones et al., 2017; Percival et al., 2017; Thibodeau and Bergquist, 2017; Bond and Grasby, 2020; review in Grasby et al., 2019; Keller et al., 2020). Similarly, three submarine LIPs have been identified as active during the Cretaceous Oceanic Anoxic Events (OAEs) (e.g., Aptian OAE1a, Aptian-Albian OAE1b, Cenomanian-Turonian OAE2, Valanginian, Toarcian) (e.g., Charbonnier and Föllmi, 2017; Charbonnier et al., 2017; Scaife et al., 2017; Percival et al., 2018; Them II et al., 2019; Charbonnier et al., 2020) (Fig. 4). This correlation suggests sediment deposition during times of LIPs volcanism, or any major volcanic eruptions, could be detected by Hg anomalies.

The main source of Hg to the environment is from volcanic emissions, atmospheric transport over 6 months to one year and fallout into terrestrial and marine environments. Secondary sources include natural coal combustion and scavenging by organic matter and clay in sediments. Hg in organic and clay-rich sediments thus contain a component of sequestered Hg that is normalized when TOC is >0.2 wt% (Thibodeau et al., 2016; Percival et al., 2018; review in Grasby et al., 2019; Keller et al., 2020). In Bilthana and Bhundmariya, TOC is consistently <0.05 wt% and < 0.08 wt%, respectively, which is likely due to diagenesis of organic matter as evident by tan orange and ochre outcrop colors. However, there is no indication of organic-rich clay layers in these predominantly oyster-rich limestones.

Our preliminary analyses from the late Cenomanian at Bilthana reveal Hg concentrations are stable and average 8–9 ppb (detection limit <3 ppb), except for a significant peak of 30 ppb in the sandy Limestone with oysters (sample 8, Fig. 4). The peak concentration suggests a volcanic eruption, which may or may not be of LIP origin. The consistently high values (8–9 ppb) suggest a significant contribution from terrestrial runoff. At Bhundmariya, Hg values are generally low (<3 ppb), likely due to greater distance from terrestrial sources, as also suggested by marly Limestone compared with sandy Limestone at Bilthana. However, the increased concentration to 6 ppb at the top could reflect increased terrestrial runoff and/or volcanic eruptions.

6. Discussion

This study began with a single objective: a routine biostratigraphic age analysis based on planktic foraminifera of the Bilthana section in Gujarat. It turned out to be a high-stress nearly monospecific assemblage in an estuarine to subtidal environment of late Cenomanian age. We confirmed this observation by collecting and analyzing a second

locality, Bhundmariya located ~25 km to the east (Fig. 1C). Results showed deposition at Bhundmariya occurred in slightly deeper subtidal waters with higher species diversity and good index species (*W. archaeocretacea, D. imbricata, D. hagni*) for the late Cenomanian correlative with the OAE2.

With this new information, we added objective-2: evaluate the onset of the sea-level transgression based on sediments and fossil assemblages. At Bilthana and Bhundmariya, the Nimar and Micritic Sandstones at the base of the Bagh Group overlie Precambrian Archean rocks from Gujarat in the west to Madhya Pradesh in the east. In the western Narmada Basin, few benthic and planktic brackish water foraminifera are present along with ostracods and calcareous algae of late Cenomanian age (Table 1), thus demonstrating that the first sea-level transgression began in late Cenomanian sands and reached peak in oyster beds or biostromes at Bilthana. As the transgression progressed, oyster biostromes drowned giving way to sandy Limestone with oysters (Fig. 4).

At Bhundmariya, oyster beds are absent but similar low diversity assemblages (2–3 species) overlie the sandstones in the first 1.5 m of the marly Limestone with oysters. Upsection, planktic foraminifera diversified rapidly with larger species and index species characteristic of the OAE2 (*W. archaeocretacea, D. imbricata, D. hagni*), suggesting rapid deepening to shallow neritic depths (Fig. 5). Thus, we concluded that the sea-level transgression into the Narmada Basin began in the late Cenomanian at the time of the OAE2.

This conclusion led us to objective-3: testing the link between the sea-level transgression and the OAE2 based on carbon isotopes, and environmental changes based on oxygen isotopes. In Bilthana and Bhundmariya, the $\delta^{18}O$ records, reveal intervals of very negative values indicative of fresh water runoff from land areas, which affected all species intolerant of brackish water environments (Figs. 4, 5).

At Bilthana, the $\delta^{13}C$ excursion began in the sandstones above the Archean rocks and reached the excursion peak in the oyster beds (Fig. 4), decreased by 2‰ and rebounded. At Bhundmariya, the $\delta^{13}C$ excursion was recorded in the marly Limestone with oysters, with results similar to the characteristic prolonged plateau with gradual decrease and fluctuating values after the OAE2 $\delta^{13}C$ excursion peak. We concluded that the outcrops in both sections contain partial OAE2 records.

We compared these records with the GSSP at Pueblo, Colorado, USA, and the Wadi El Ghaib section in the Sinai, Egypt, which have the globally characteristic OAE2 $\delta^{13}C$ excursions (Fig. 6). This comparison is also based on planktic foraminifera biostratigraphy. The $\delta^{13}C$ record from Bilthana reveals presence of the $\delta^{13}C$ excursion gradual increase and peak, plus the partial presence of the subsequent plateau. At Bhundmariya, both the plateau and gradual decrease are present. The $\delta^{13}C$ excursion peak is missing, supported by the faunal assemblages indicating erosion or non-deposition. The comparison of the OAE2 $\delta^{13}C$ excursion in the Gujarat sections with Pueblo and Wadi El Ghaib is based on biostratigraphy and indicates this excursion is partially present and can be recognized even though the sequences are incomplete.

Last, we tested objective-4: the potential link between volcanism, based on mercury fallout, and mercury toxicity during this time. Mercury concentrations at Bilthana are relatively stable averaging 8–9 ppb, three times the detection limit, which likely indicates terrestrially enriched Hg runoff. There is one significant peak of 30 ppb, indicative of a larger volcanic eruption possibly from one of the LIPs associated with the OAE2 (Caribbean Plateau, Ontong-Java Plateau, Madagascar Province (Ernst, 2014). At Bhundmariya, Hg values are generally at or below the detection limit of 3 ppb and reach 6 ppb at the top. However, the record is incomplete and inconclusive. Toxicity based on Hg cannot be evaluated in these shallow, estuarine environments, where the major limiting factor for planktic and benthic foraminifera is fresh water influx from land that significantly reduced abundance and diversity.

In summary, given the data and its limitations, we conclude the Narmada Seaway began in Gujarat with the sea-level transgression during the late Cenomanian and progressed eastward towards Madhya

Pradesh during the Turonian through Coniacian and Santonian as indicated by current fossil data and biostratigraphy (Fig. 7A). Our preliminary analyses of Turonian-Coniacian-Santonian sequences suggest that by this time the Narmada Seaway deepened to a middle neritic environment. Consequently, the Narmada Seaway must have existed by the end of the Maastrichtian, possibly as a shallower seaway as cooling persisted from the Campanian into the late Maastrichtian. By early Danian, the presence of early Danian planktic foraminifera in shallow intertrappeans at Jhilmili suggests the end of the maximum extent of this seaway (Fig. 7B) (Keller et al., 2009).

A recent review of the India seaways based on tectonic history and some fossil groups concluded there was inconclusive evidence the Narmada Seaway existed by the end of the Cretaceous (Kumari et al., 2020). Instead, they proposed the Godavari rift basin as the only inland seaway at this time. We concur that the Godavari Seaway must have existed during the late Cretaceous and could have connected with the Narmada Seaway and formed the Trans-India Seaway (Fig. 7A).

A recent study also reported organic-rich sediments of the late Cenomanian to early Turonian from subsurface cores in the Cauvery Basin of south India, correlative with the global transgression and the OAE2 (Nagendra and Reddy, 2017). In this area, sedimentation occurred in a middle-neritic environment marked by high concentrations of dark colored pyritized agglutinated foraminifera and dwarfed calcareous benthic foraminifera (e.g., *Lenticulina, Gavelinella*), which indicate high-stress dysoxic to anoxic environments (Govindan, 1993). Organic-rich shale deposition continued into the early Turonian correlative with the transgression and expansion of oxygen-depleted waters into shallower neritic environments (Nagendra and Reddy, 2017). The Cauvery River basin thus also recorded the Cenomanian-Turonian transgression, just as the Godavari and Krishna River basins in the Rajahmundry area and the Narmada River in the north. India's entire south-eastern seaboard must have been inundated by the Cenomanian-Turonian transgression (Fig. 7B).

We suggest that the Godavari and Narmada Seaways likely coexisted. The Narmada Seaway across central India and the Godavari Seaway from Rajahmundry north to Nagpur may have connected at times with the Narmada Seaway via the Narmada-Tapti rift zone and formed a Trans-India Seaway (Fig. 7B, C).

The global sea-level rise during the late Cenomanian to early Turonian thus inundated low-lying areas worldwide and created shallow carbonate seas and vast inland seaways, such as the Trans-Sahara Seaway (Meister et al., 1992; Pascal et al., 1993) and the US Western Inland Seaway spanning from the Gulf of Mexico to the polar area (Fig. 7C) (e.g., Haq et al., 1987; Hallam, 1992; Haq, 2014). In southern India's Cauvery Basin, sea-level transgressions have been identified for nearly all of the Cretaceous Oceanic Anoxic Events (OAEs) (review in Nagendra and Reddy, 2017).

6.1. Global context of OAE2

Placing the Cenomanian-Turonian OAE2, the $\delta^{13}C$ excursion, climate change, sea-level transgression, evolution and extinctions into the global context helps understand this complex time interval (Fig. 8). The Cretaceous was a time of rapid greenhouse warming and cooling episodes, rising sea-levels and repeated platform drowning, accompanied by major carbon isotope excursions, episodic OAEs, and increased volcanic activity from LIPs. The largest of the anoxic events is OAE2, which occurred during the late Cenomanian to early Turonian ~94–90 Ma at a time of LIP eruptions in the Caribbean, Ontong Java and Madagascar (Fig. 8) (Ernst, 2014; Scaife et al., 2017).

By the late Cenomanian to early Turonian, climate warmed and reached peak sea-surface (SS) temperatures of 28 °C during OAE2 (Huber et al., 1995; Weissert and Erba, 2004; Jarvis et al., 2006, Jarvis et al., 2011; Keller, 2008), interrupted by short-term cooling (Plenus marl) (O'Connor et al., 2020). From the early Turonian through the Santonian SS temperatures remained high ~25 °C interrupted by cooling
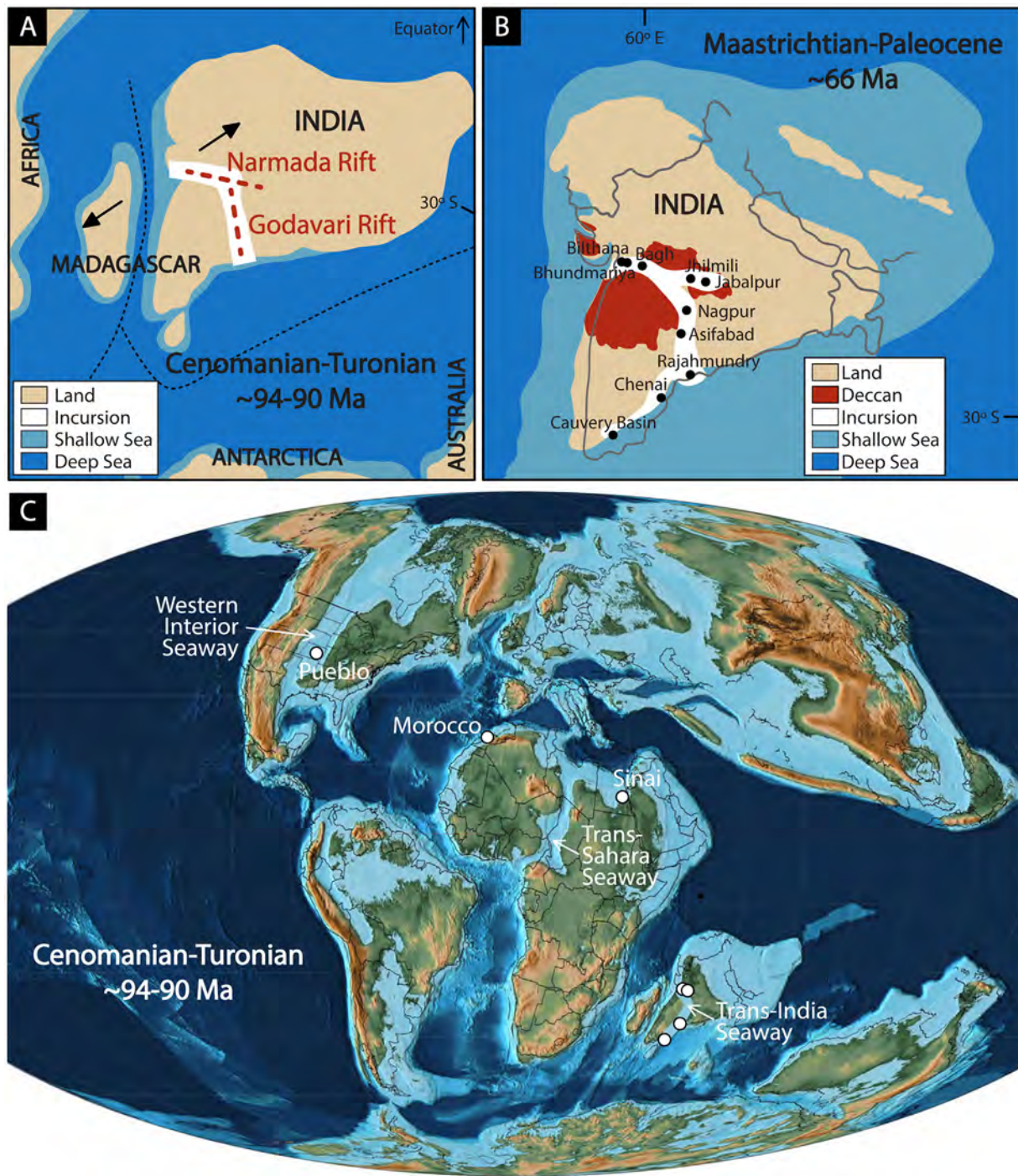
Fig. 7. Paleomaps of India. (A) The late Cenomanian-early Turonian paleomap showing the western Narmada Seaway incursion (modified from Kumari et al., 2020). (B) The Maastrichtian-Paleocene paleomap shows the Narmada and Godavari Seaways. These two seaways may have been joined through the Tapti-Narmada rift zone (modified from Kumari et al., 2020). (C) Global late Cenomanian-early Turonian paleomap showing the numerous incursions and seaways associated to a global transgression (modified from Scotese, 2014).

episodes to ~20 °C (Fig. 8). Warmer SS temperatures for OAE2 have been estimated based on TEX$_{86}$ from the Cassis section in southern France where temperatures reached highs of 38 °C during the $\delta^{13}C$ excursion and lows of 32 °C during the Plenus cool event (Heimhofer et al., 2018).

During the OAE2, the sea-level reached 250–300 m above the present level, inundating carbonate platforms and continental shelf areas and forming vast inland seas, including the USA Western Interior Seaway spanning from the Gulf of Mexico to the Arctic (Gale et al., 2008), the Trans-Sahara Seaway of North Africa and now also the Trans-India

Seaway combining the Narmada and Godavari Seaways (Fig. 7C). A major CIE accompanied this sea-level transgression in open marine, shallow carbonate platform environments and inland seaways. This $\delta^{13}C$ excursion defines the OAE2 that occurred in four distinct phases: (1) the gradual increase, (2) the excursion peak associated with the Plenus Cold Event, (3) the plateau, and (4) the gradual decrease to normal values in the early Turonian. These $\delta^{13}C$ excursion characteristics are globally identifiable from estuarine-subtidal to deep-sea environments (Fig. 6). They are the $\delta^{13}C$ fingerprint of the OAE2 and an
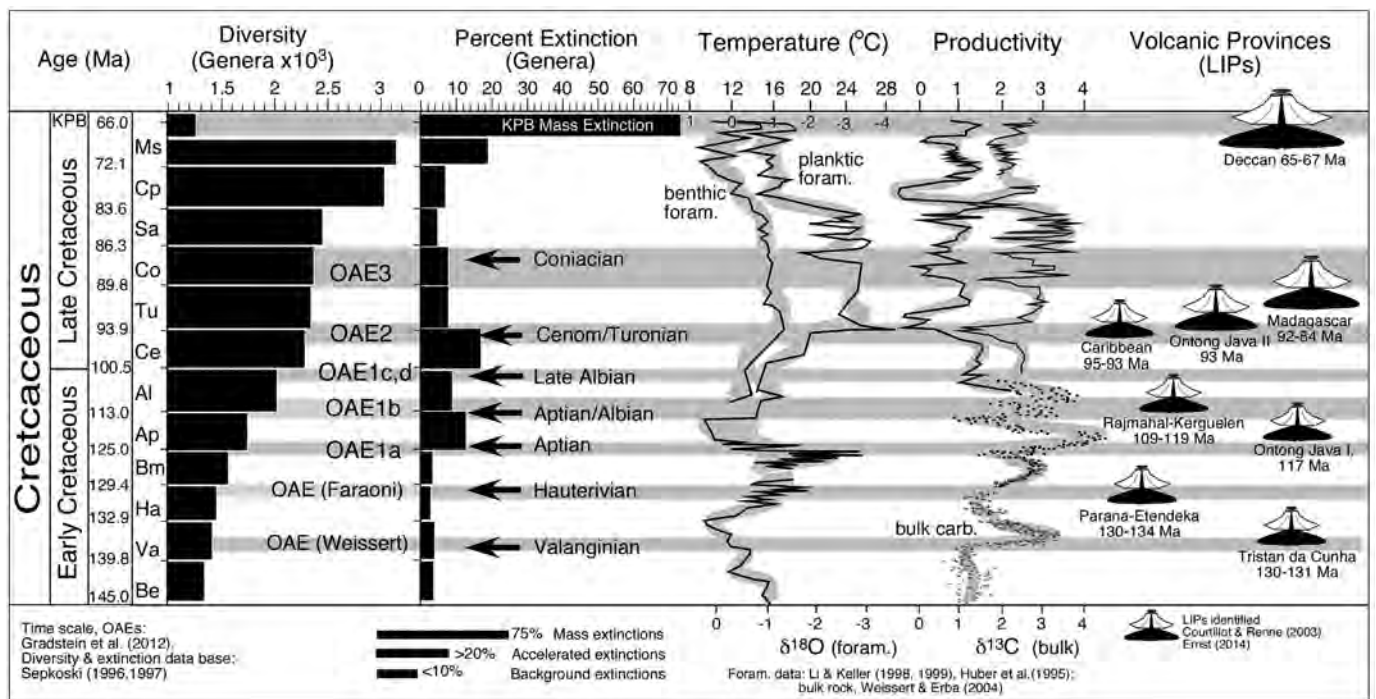
Fig. 8. Summary of Cretaceous oceanic anoxic events (OAEs), climate (δ^{18}O) and bioproductivity (δ^{13}C) changes (Huber et al., 1995; Li and Keller, 1998, 1999; Weissert and Erba, 2004), increasing planktic foraminiferal diversity through the Cretaceous and absence of accelerated extinctions by genera (Sepkoski Jr., 1996; Sepkoski Jr., 1997). Three Large Igneous Provinces (LIPs) are associated with the time of OAE2 (Courtillot and Renne, 2003; Ernst, 2014). Ages based on time scale by Gradstein et al. (2012). The late Cenomanian OAE2 began with a major sea-level transgression accompanied by ~8 °C climate warming and 2‰ increased productivity associated with black shale deposition. The western India interior seaway of the Narmada Valley began with this sea level transgression during the late Cenomanian (modified from Keller, 2008).

excellent correlation tool from open marine to the Inland Seaway (Jarvis et al., 2011; Wendler, 2013; O'Connor et al., 2020).

Despite these major global environmental changes, there was no mass extinction in marine life and no significantly increased extinctions in genera. Diversity in invertebrate genera increased gradually through the Cretaceous OAEs, reached a plateau between the Cenomanian to Santonian and peaked in the Campanian and Maastrichtian prior to the KPB mass extinction (Fig. 8). Extinctions remained in background values (<10%), but slightly accelerated between the Aptian and Cenomanian OAEs and increased during the Maastrichtian prior to the KPB mass extinction (Sepkoski Jr., 1996; Sepkoski Jr., 1997). However, the species record shows relatively few extinctions in planktic foraminifera or ammonites (Keller and Pardo, 2004; Monnet, 2009), but rapid evolution and/or adaptation of survivor species to the changing high-stress environments associated with OAE2 and submarine LIP eruptions (e.g., salinity, low oxygen, high productivity, temperature changes) (Scaife et al., 2017). In contrast, all five mass extinctions in Earth's history are associated with continental flood basalts LIPs, which globally resulted in rapid climate changes, distribution of toxins via the atmosphere causing adverse effects, and terrestrial acidity and toxicity (Grasby et al., 2020).

7. Conclusions

(1) We report the first evidence of the late Cenomanian-early Turonian OAE2 in the western Narmada Basin associated with the largest sea-level transgression of the Cretaceous that initiated the western Narmada Seaway, which by the end of the Turonian reached from Gujarat through Madhya Pradesh. At times this seaway may have connected to the Godavari Seaway via the Narmada-Tpati rift forming a Trans-India Seaway to Rajahmundry.

(2) The characteristic OAE2 gradual onset of the δ^{13}C excursion began with the transgression and peaked in the oyster beds or

biostromes at Bilthana in a subtidal to estuarine environment. The δ^{13}C plateau followed in the overlying Limestone with oysters.

(3) The onset of the transgression is recognized in the Nimar Sandstone and Micritic Sandstone by an influx of few benthic and planktic foraminifera and ostracods indicative of the late Cenomanian.

(4) The OAE2 δ^{13}C excursion at Gujarat is dated based on planktic foraminifera biozones and correlated with the GSSP at Pueblo, Colorado, USA, and the Wadi El Ghaib section in the Sinai, Egypt.

(5) Very negative δ^{18}O values (−7 to −8‰) indicate episodic terrestrial fresh water influx associated with high-stress, planktic foraminiferal assemblages dominated by nearly monospecific *Muricohedbergella* species (*M. delrioensis*) tolerant of salinity fluctuations and brackish water benthic foraminifera.

(6) The deepening transgression during the late Cenomanian δ^{13}C plateau is marked by increased species diversity, with common *Whiteinella* and few *Dicarinella* characteristic of the latest Cenomanian *W. archaeocretacea* zone. Similar faunal progressions mark this global sea-level transgression from Egypt to Morocco and the USA Western Interior Seaway.

Supplementary data to this article can be found online at https://doi.org/10.1016/j.gr.2021.02.013.

Author Contributions

Gerta Keller: Conceptualization; Data curation; Formal analysis; Funding acquisition; Investigation; Methodology; Project administration; Resources; Supervision; Validation; Visualization; Writing - original draft; Writing - review & editing. **Madan Nagori:** Funding acquisition; Investigation; Methodology; Resources; Writing - review & editing. **Maya Chaudhary:** Investigation; Methodology; Resources; Writing - review & editing. **Nallapa A. Reddy:** Investigation;

Declaration of Competing Interest

The authors declare that they have no known competing financial interests or personal relationships that could have appeared to influence the work reported in this paper.

Acknowledgements

References

Bansal, U., Banerjee, S., Pande, K., Ruidas, D.K., 2020. Unusual seawater composition of the late cretaceous Tethys imprinted in glauconite of Narmada basin, Central India. Geol. Mag. 157, 233–247. https://doi.org/10.1017/S0016756819000621.

Biswas, S.K., 1987. Regional tectonic framework structure and evolution of western marginal basins of India. Tectonophysics 135, 307–327. https://doi.org/10.1016/0040-1951(87)90115-6.

Bomou, B., Adatte, T., Tantawy, A., Mort, H., Fleitmann, D., Huang, Y., Föllmi, K.B., 2013. The expression of the Cenomanian–Turonian oceanic anoxic event in Tibet. Palaeogeogr. Palaeoclimatol. Palaeoecol. 369, 466–481. https://doi.org/10.1016/j.palaeo.2012.11.011.

Bond, D.P.G., Grasby, S.E., 2020. Late Ordovician mass extinction caused by volcanism, warming, and anoxia, not cooling and glaciation. Geology 48. https://doi.org/10.1130/G47377.1.

Caron, M., Dall'Agnolo, S., Accarie, H., Barrera, E., Kauffman, E.G., Amedro, F., Robaszynski, F., 2006. High-resolution stratigraphy of the Cenomanian-Turonian boundary interval at Pueblo (USA) and Wadi Bahloul (Tunisia): stable isotope and bio-events correlation. Geobios 39, 171–200. https://doi.org/10.1016/j.geobios.2004.11.004.

Charbonnier, G., Föllmi, K.B., 2017. Mercury enrichments in lower Aptian sediments support the link between Ontong Java large igneous province activity and oceanic anoxic episode 1a. Geology 45, 63–66. https://doi.org/10.1130/G38207.1.

Charbonnier, G., Morales, C., Duchamp-Alphonse, S., Westermann, S., Adatte, T., Föllmi, K.B., 2017. Mercury enrichment indicates volcanic triggering of Valanginian environmental change. Sci. Rep. 7, 40808. https://doi.org/10.1038/srep40808.

Charbonnier, G., Adatte, T., Follmi, K.B., Guillaume, S., 2020. Effect of intense weathering and postdepositional degradation of organic matter on Hg/TOC Proxy in organic-rich sediments and its implications for deep-time investigations. Geochem. Geophys. Geosyst. 21, e2019GC008707. https://doi.org/10.1029/2019GC008707.

Chatterjee, S., Goswami, A., Scotese, C.R., 2013. The longest voyage: Tectonic, magmatic, and paleoclimatic evolution of the Indian plate during its northward flight from Gondwana to Asia. Gondwana Res. 23, 238–267. https://doi.org/10.1016/j.gr.2012.07.001.

Chaudhary, M., Nagori, M.L., 2019. Ostracods from the Bagh formation (Upper cretaceous) of the Narmada Basin, India: their age and paleobiogeographical significance. Micropaleontology 65, 513–543.

Chaudhary, M., Nagori, M.L., Bhanat, N., 2017a. Palaeobiogeographic implications of Ostracoda: a case study from Bagh formation (Upper cretaceous) of Narbada valley, Madhya Pradesh and Gujarat. Indian J. Appl. Res. 7, 316–319. https://doi.org/10.36106/ijar.

Chaudhary, M., Nagori, M.L., Bhanat, N., 2017b. Cytherelloidea (ostracoda) from the Upper cretaceous Bagh Formation of Madhya Pradesh, India: its affinity and palaeogeographic implications. J. Paleontol. Soc. India 62, 217–224.

Chaudhary, M., Nagori, M.L., Khosla, S.C., 2019. Ostracod genus Rostrocytheridea from the Bagh Formation (Upper cretaceous) of Narmada Basin, Madhya Pradesh and Gujarat, India. J. Paleontol. Soc. India 64, 73–82.

Chiplonkar, G.W., 1982. Bagh Beds-their stratigraphy, faunas, age and affinities and environment of deposition – A review. Presidential Address: Proceedings of the 69th session Indian Science Congress, Mysore, Geology, Section, Part 2, pp. 1–22.

Courtillot, V.E., Renne, P.R., 2003. On the ages of flood basalt events. Compt. Rendus Geosci. 335, 113–140. https://doi.org/10.1016/S1631-0713(03)00006-3.

El-Sabbagh, A.M., Tantawy, A.A., Keller, G., Khozyem, H.M., Spangenberg, J., Adatte, T., Gertsch, B., 2011. Stratigraphy of the Cenomanian-Turonian Oceanic Anoxic Event OAE2 in shallow shelf sequences of NE Egypt. Cretac. Res. 32, 705–722. https://doi.org/10.1016/j.cretres.2011.04.006.

Ernst, R.E., 2014. Large Igneous Provinces. Cambridge University Press, Cambridge https://doi.org/10.1017/CBO9781139025300.

Gale, A.S., Voigt, S., Sageman, B.B., Kennedy, W.J., 2008. Eustatic sea-level record for the Cenomanian (late cretaceous) – Extension to the Western Interior Basin, USA. Geology 36, 859–862. https://doi.org/10.1130/G24838A.1.

Gangopadhyay, T.K., Bardhan, S., 2007. Ornamental polymorphism in Placenticeraskaffrarium (Ammonoidea; Upper cretaceous of India): Evolutionary implications. In: Landman, N.H., Davis, R.A., Maps, R.H. (Eds.), Cephalopods Present and Past: New Insights and Fresh Perspectives. Springer, pp. 97–120 https://doi.org/10.1007/978-1-4020-6806-5_5.

Gertsch, B., Keller, G., Adatte, T., Berner, Z., Tantawy, A.A., Kassab, A.S., El-Sabbagh, A.M., Mort, H.P., Stueben, D., 2008. Cenomanian-Turonian transition in shallow water sequences of the Sinai, Egypt. Int. J. Earth Sci. 99, 165–182. https://doi.org/10.1007/s00531-008-0374-4.

Gertsch, B., Keller, G., Adatte, T., Berner, Z., Tantawy, A.A., El-Sabbagh, A.M., Mort, H.P., Stueben, D., 2010. Middle and late Cenomanian anoxic events in shallow shelf environments of western Morocco. Sedimentology 57, 1430–1462. https://doi.org/10.1111/j.1365-3091.2010.01151.x.

Ghosh, P., Bhattacharya, S.K., Jani, R.A., 1995. Palaeoclimate and palaeovegetation in Central India during the Upper cretaceous based on stable isotopic composition of the palaeosol carbonates. Palaeogeogr. Palaeoclimatol. Palaeoecol. 114, 285–296. https://doi.org/10.1016/0031-0182(94)00082-J.

Gong, Q., Wang, X., Zhao, L., Grasby, S.E., Chen, Z.Q., Zhang, L., Li, Y., Cao, L., Li, Z., 2017. Mercury spikes suggest volcanic driver of the Ordovician-Silurian mass extinction. Sci. Rep. 7, 5304. https://doi.org/10.1038/s41598-017-05524-5.

Govindan, A., 1993. Cretaceous anoxic events, sea level changes and microfauna in Cauvery Basin, India. Proc. Second Semin. Petrolif. Basins India 1, 161–176.

Gradstein, F.M., Ogg, G., Schmitz, M., 2012. The Geologic Time Scale. Elsevier, Amsterdam https://doi.org/10.1016/C2011-1-08249-8.

Grasby, S.E., Beauchamp, B., Bond, D.P.G., Wignall, P.B., Sanei, H., 2016. Mercury anomalies associated with three extinction events (Capitanian Crisis, latest Permian Extinction and the Smithian/Spathian Extinction) in NW Pangea. Geol. Mag. 153, 285–297. https://doi.org/10.1017/S0016756815000436.

Grasby, S.E., Them II, T.R., Chen, Z., Yin, R., Ardakani, O.H., 2019. Mercury as a proxy for volcanic emissions in the geologic record. Earth Sci. Rev. 196, 102880. https://doi.org/10.1016/j.earscirev.2019.102880.

Grasby, S.E., Liu, X., Yin, R., Ernst, R.E., Chen, Z., 2020. Toxic mercury pulses into late Permian terrestrial and marine environments. Geology 48, 830–833. https://doi.org/10.1130/G47295.1.

Hallam, A., 1992. Phanerozoic Sea-Level Changes. Columbia University Press.

Haq, B.U., 2014. Cretaceous eustasy revisited. Glob. Planet. Chang. 113, 44–58. https://doi.org/10.1016/j.gloplacha.2013.12.007.

Haq, B.U., Hardenbol, J., Vail, P.R., 1987. Chronology of fluctuating sea levels since the Triassic (250 million years ago to present). Science 235, 1156–1167. https://doi.org/10.1126/science.235.4793.1156.

Heimhofer, U., Wucherpfennig, N., Adatte, T., Schouten, S., Schneebeli-Hermann, E., Gardin, S., Keller, G., Kujau, A., 2018. Vegetation response to exceptional warmth during Oceanic Anoxic Event 2. Nat. Commun. 9, 3832. https://doi.org/10.1038/s41467-018-06319-6.

Huber, B.T., Hodell, D.A., Hamilton, C.P., 1995. Middle-late cretaceous climate of the southern high latitudes: stable isotopic evidence for minimal equator-to-pole thermal gradients. Geol. Soc. Am. Bull. 107, 1164–1191. https://doi.org/10.1130/0016-7606(1995)107<1164:MLCCOT>2.3.CO;2.

Jain, S.P., 1961. Discovery of Ostracoda and smaller Foraminifera from the Upper cretaceous Bagh Beds, M.P. Curr. Sci. 39, 341–342.

Jain, S.P., 1975. Ostracoda from the Bagh Beds (Upper cretaceous) of Madhya Pradesh. Geophytology 5, 188–212.

Jaitley, A.K., Ajane, R., 2013. Comments on Placenticeras mintoi (Vredenburg, 1906) from the Bagh Beds (late cretaceous), Central India with special reference to Turonian Nodular Limestone Horizon. J. Geol. Soc. India 81, 565–574. https://doi.org/10.1007/s12594-013-0072-0.

Jarvis, I., Gale, A.S., Jenkyns, H.C., Pearce, M.A., 2006. Secular variation in Late Cretaceous carbon isotopes and sea-level change: Evidence from a new d13C carbonate reference curve for the Cenomanian–Campanian (99.6–70.6 Ma). Geological Magazine 143, 561–608. https://doi.org/10.1017/S0016756806002421.

Jarvis, I., Lignum, J.S., Gröcke, D.R., Jenkyns, H.C., Pearce, M.A., 2011. Black shale deposition, atmospheric CO2 drawdown, and cooling during the Cenomanian-Turonian Oceanic Anoxic Event. Paleoceanogr. Paleoclimatol. 26, PA3201. https://doi.org/10.1029/2010PA002081.

Jones, D.S., Martini, A.M., Fike, D.A., Kaiho, K., 2017. A volcanic trigger for the late Ordovician mass extinction? Mercury data from South China and Laurentia. Geology 45, 631–634. https://doi.org/10.1130/G38940.1.

Keller, G., 2003. Biotic effects of volcanism and impacts. Earth Planet. Sci. Lett. 215, 249–264. https://doi.org/10.1016/S0012-821X(03)00390-X.

Keller, G., 2008. Cretaceous climate, volcanism, impacts and biotic effects. Cretac. Res. 29, 754–771. https://doi.org/10.1016/j.cretres.2008.05.030.

Keller, G., Abramovich, S., 2009. Lilliput effect in late Maastrichtian planktic Foraminifera: Response to Environmental stress. Paleogeogr. Paleoclimatol. Paleoecol. 271, 52–68. https://doi.org/10.1016/j.palaeo.2009.08.029.

Keller, G., Pardo, A., 2004. Paleoecology of the Cenomanian-Turonian Stratotype Section (GSSP) at Pueblo, Colorado. Mar. Micropaleontol. 51, 95–128.

Keller, G., Han, Q., Adatte, T., Burns, S.J., 2001. Paleoenvironment of the Cenomanian-Turonian transition at Eastbourne, England. Cretac. Res. 22, 391–422.

Keller, G., Stueben, D., Berner, Z., Adatte, T., 2004. Cenomanian-Turonian δ¹³C, δ¹⁸O, sea-level and salinity variations at Pueblo, Colorado. Paleoclimatol. Paleoecol. Paleogeogr. 211, 19–43. https://doi.org/10.1016/j.palaeo.2004.04.003.

Keller, G., Adatte, T., Tantawy, A.A., Berner, Z., Stueben, D., 2007. High stress late Maastrichtian – early Danian palaeoenvironment in the Neuquen Basin, Argentina. Cretac. Res. 28, 939–960. https://doi.org/10.1016/j.cretres.2007.01.006.

Keller, G., Adatte, T., Berner, Z., Chellai, E.H., Stueben, D., 2008. Oceanic events and biotic effects of the Cenomanian-Turonian Anoxic Event, Tarfaya Basin, Morocco. Cretac. Res. 29, 976–994. https://doi.org/10.1016/j.cretres.2008.05.020.

Keller, G., Adatte, T., Bajpai, S., Khosla, A., Sharma, R., Widdowson, M., Khosla, S.C., Mohabey, D.M., Gertsch, B., Sahni, A., 2009. KT transition in Deccan Traps of Central India marks major marine seaway across India. Earth Planet. Sci. Lett. 282, 10–23. https://doi.org/10.1016/j.epsl.2009.02.016.

Keller, G., Mateo, P., Monkenbusch, J., Thibault, N., Punekar, J., Spangenberg, J.E., Abramovich, S., Ashchenazi-Poliveda, S., Schoene, B., Eddy, M.P., Samperton, K., Khadri, S.F.R., Adatte, T., 2020. Mercury linked to Deccan Traps Volcanism, climate Change and the end-cretaceous mass extinction. Glob. Planet. Chang. 194, 103312. https://doi.org/10.1016/j.gloplacha.2020.103312.

Kuhnt, W., Luderer, F., Nederbragt, S., Thurow, J., Wagner, T., 2004. Orbital-scale record of the late Cenomanian–Turonian oceanic anoxic event (OAE-2) in the Tarfaya Basin (Morocco). Int. J. Earth Sci. 94, 147–159. https://doi.org/10.1007/s00531-004-0440-5.

Kuhnt, W., Holbourn, A.E., Beil, S., Aquit, M., Tim Krawczyk, M.T., Flögel, S., Chellai, H., Jabour, H., 2017. Unraveling the onset of cretaceous Oceanic anoxic event 2 in an extended sediment archive from the Tarfaya-Laayoune Basin, Morocco. Paleoceanogr. Paleoclimatol. 32, 923–946. https://doi.org/10.1002/2017PA003146.

Kumar, S., Singh, M.P., Mohabey, D.M., 1999. Lameta and Bagh Beds, Central India: Field Guide. J. Palaeontol. Soc. India 48.

Kumar, S., Pathak, D.B., Pandey, B., Jaitly, A.K., Gautam, J.P., 2018. The age of the Nodular Limestone Formation (late cretaceous), Narmada Basin, Central India. J. Earth Syst. Sci. 127, 109. https://doi.org/10.1007/s12040-018-1017-1.

Kumari, V., Tandon, S.K., Kumar, N., Ghatak, A., 2020. Epicontinental Permian-cretaceous seaways in Central India: the debate for the Narmada versus Godavari rifts for the Cretaceous-Tertiary incursion. Earth Sci. Rev. 211, 103284. https://doi.org/10.1016/j.earscirev.2020.103284.

Kundal, P., Sanganwar, B.N., 1998. Stratigraphical, palaeogeographical and palaeoenvironmental significance of fossil calcareous algae from Nimar Sandstone Formation, Bagh Group (Cenomanian–Turonian) of Pipaldehla, Jhabua Dt, MP. Curr. Sci. 75, 702–708. https://www.jstor.org/stable/24101717.

Leckie, R.M., 1987. Paleoecology of mid-cretaceous planktic foraminifera: a comparison of open ocean and epicontinental sea assemblages. Micropaleontology 33, 164–176. https://doi.org/10.2307/1485491.

Leckie, R.M., Yuretich, R.F., West, L.O.L., Finkelstein, D., Schmidt, M., 1998. Paleoceanography of the southwestern Interior Sea during the time of the Cenomanian–Turonian boundary (late Cretaceous). In: Dean, W.E., Arthur, M.A. (Eds.), Concepts in Sedimentology and Paleontology. 6. SEPM Society for Sedimentary Geology, pp. 101–126. https://doi.org/10.2110/csp.98.06.0101.

Li, L., Keller, G., 1998. Abrupt deep-sea warming at the end of the cretaceous. Geology 26, 995–998. https://doi.org/10.1130/0091-7613(1998)026<0995:ADSWAT>2.3.CO;2.

Li, L., Keller, G., 1999. Variability in late cretaceous climate and deep waters: evidence from stable isotopes. Mar. Geol. 161, 171–190. https://doi.org/10.1016/S0025-3227(99)00078-X.

Marshall, J.D., 1992. Climatic and oceanographic isotopic signals from the carbonate rock record and their preservation. Geol. Mag. 129, 143–160. https://doi.org/10.1017/S0016756800008244.

Meister, C., Allzuma, K., Mathey, B., 1992. Les ammonites du Niger (Afrique occidentale) et la Transgression Trans-saharienne au cours du CenomanieneTuronien. Geobios 25, 55–100. https://doi.org/10.1016/S0016-6995(09)90038-9.

Monnet, C., 2009. The Cenomanian–Turonian boundary mass extinction (late cretaceous): New insights from ammonoid biodiversity patterns of Europe, Tunisia and the WesternInterior (North America). Paleogeogr. Paleoclimatol. Paleoecol. 282, 88–104. https://doi.org/10.1016/j.palaeo.2009.08.014.

Nagendra, R., Reddy, A.N., 2017. Major geologic events of the Cauvery Basin, India and their correlation with global signatures - a review. J. Paleogeogr. 6, 69–83. https://doi.org/10.1016/j.jop.2016.09.002.

Nayak, K.K., 1987. Foraminifera from the Nimar Sandstone of Bagh Beds, Jhabua District, Madhya Pradesh. Biovigyanam 13, 30–39.

O'Connor, L.K., Jenkyns, H.C., Robinson, S.A., Remmelzwaal, S.R.C., Batenburg, S.J., Parkinson, I.J., Gale, A.S., 2020. A re-evaluation of the Plenus Cold Event, and the links between CO2, temperature, and seawater chemistry during OAE 2. Paleoceanogr. Paleoclimatol. 35, e2019PA003631. https://doi.org/10.1029/2019PA003631.

Pascal, A.F., Mathey, B.J., Alzuma, K., Lang, L., Meister, C., 1993. Late Cenomanian–early Turonian shelf ramp, Niger, West Africa. In: Simo, A.J., Scott, R.W., Masse, J.P. (Eds.), Cretaceous Carbonate Platforms. 56. American Association of Petroleum Geologists Memoir, pp. 145–154. https://doi.org/10.1306/M56578C12.

Percival, L.M.E., Ruhl, M., Hesselbo, S.P., Jenkyns, H.C., Mather, T.A., Whiteside, J.H., 2017. Mercury evidence for pulsed volcanism during the end-Triassic mass extinction. Proc. Natl. Acad. Sci. 114, 7929–7934. https://doi.org/10.1073/pnas.1705378114.

Percival, L.M.E., Jenkyns, H.C., Mather, T.A., Dickson, A.J., Batenburg, S.J., Ruhl, M., Hesselbo, S.P., Barclay, R., Jarvis, I., Robinson, S.A., Woelders, L, 2018. Does large Igneous Province volcanism always perturb the mercury cycle? Comparing the records of Oceanic Anoxic event 2 and the end-cretaceous to other Mesozoic events. Am. J. Sci. 318, 799–860. https://doi.org/10.2475/08.2018.01.

Pratt, L.M., 1984. Influence of paleoenvironmental factors on the preservation of organic matter in middle cretaceous Greenhorn Formation near Pueblo, Colorado. Am. Assoc. Pet. Geol. Bull. 68, 1146–1159. https://doi.org/10.1306/AD4616E7-16F7-11D7-8645000102C1865D.

Pufahl, P.K., James, N.P., 2006. Monospecific Pliocene oyster buildups, Murray Basin, South Australia: brackish water end member of the reef spectrum. Palaeogeogr. Palaeoclimatol. Palaeoecol. 233, 11–33. https://doi.org/10.1016/j.palaeo.2005.09.015.

Rajshekhar, C., 1987. Foraminifera from Nimar Sandstone, Bagh beds, Madhya Pradesh, India. Biovigyanam 8, 89–97.

Rajshekhar, C., 1995. Foraminifera from the Bagh group, Narmada Basin, India. J. Geol. Soc. India 46, 413–428.

Rajshekhar, C., Atpalkar, S., 1995. Foraminifera from the Nodular limestone, Bilthana, Gujarat: Stratigraphic significance. J. Geol. Soc. India 45, 585–593.

Scaife, J.D., Ruhl, M., Dickson, A.J., Mather, T.A., Jenkyns, H.C., Percival, L.M.E., Hesselbo, S.P., Cartwright, J., Eldrett, J.S., Bergman, S.C., Minisini, D., 2017. Sedimentary mercury enrichments as a marker for sub-marine large Igneous province volcanism? Evidence from the Mid-Cenomanian Event and Oceanic Anoxic Event 2 (Late Cretaceous). Geochem. Geophys. Geosyst. 18, 4453–4475. https://doi.org/10.1002/2017GC007153.

Schrag, D.P., DePaolo, D.J., Richter, F.M., 1995. Reconstructing past sea surface temperatures: correcting for diagenesis of bulk marine carbon. Geochim. Cosmochim. Acta 59, 2265–2278. https://doi.org/10.1016/0016-7037(95)00105-9.

Scotese, C.R., 2014. Atlas of Late Cretaceous Paleogeographic Maps, PALEOMAP Atlas for ArcGIS, volume 2, The Cretaceous, Maps 16–22, Mollweide Projection. PALEOMAP Project, Evanston, IL https://doi.org/10.13140/2.1.4691.3284.

Sepkoski Jr., J.J., 1996. Patterns of Phanerozoic extinction: A perspective from global data bases. In: Walliser, O.H. (Ed.), Global Events and Event Stratigraphy in the Phanerozoic. Springer, Berlin, Heidelberg, pp. 35–52 https://doi.org/10.1007/978-3-642-79634-0_4.

Sepkoski Jr., J.J., 1997. Biodiversity: past, present and future. J. Paleontol. 71, 35–52. https://doi.org/10.1017/S0022336000040026.

Singh, P., 1997. Ostracoda from the subsurface cretaceous strata of Manhera Tibba well-I and Shahgarh well-B, Jaisalmer basin, Rajasthan, India with special remarks on Foraminiferids. Geosci. J. 18, 1–57.

Tandon, S.K., 2000. Spatio-temporal patterns of environmental changes in late cretaceous sequences of Central India. In: Okada, H., Mateer, N.J. (Eds.), Developments in Palaeontology and Stratigraphy. 17, pp. 225–241. https://doi.org/10.1016/S0920-5446(00)80035-7.

Them II, T.R., Jagoe, C.H., Caruthers, A.H., Gilld, B.C., Grasby, S.E., Gröckef, D.R., Yin, R., Owens, J.D., 2019. Terrestrial sources as primary delivery mechanism of mercury to the oceans across the Toarcian Anoxic Event (early Jurassic). Earth Planet. Sci. Lett. 507, 62–72. https://doi.org/10.1016/j.epsl.2018.11.029.

Thibodeau, A.M., Bergquist, B.A., 2017. Do mercury isotopes record the signature of massive volcanism in marine sedimentary records? Geology 45, 95–96. https://doi.org/10.1130/focus012017.1.

Thibodeau, A.M., Ritterbush, K., Yager, J.A., West, J.A., Ibarra, Y., Berelson, W.M., Bergquist, B.A., Corsetti, F.A., 2016. Mercury anomalies and the timing of biotic recovery following the end-Triassic mass extinction. Nat. Commun. 7, 11147. https://doi.org/10.1038/ncomms11147.

Tripathi, S.C., 2005. Geological and palaeoenvironmental appraisal of Maastrichtian Lameta sediment of lower Narmada Valley, Western India and their regional correlation. Gondwana Geol. Magaz. 8, 29–35.

Tripathi, S.C., 2006. Geology and evolution of the cretaceous Infratrappean basins of lower Narmada valley, western India. J. Geol. Soc. India 67, 459–468.

Tsikos, H., Jenkyns, H.C., Walsworth-Bell, B., Petrizzo, M.R., Forster, A., Kolonic, S., Erba, E., Premoli Silva, I., Baas, M., Wagner, T., Sinninghe Damste, J.S., 2004. Carbon-isotope stratigraphy recorded by the Cenomanian–Turonian oceanic anoxic event: correlation and implications based on three key localities. J. Geol. Soc. 161, 711–719. https://doi.org/10.1144/0016-764903-077.

Weissert, H., Erba, E., 2004. Volcanism, CO2 and palaeoclimate: a late Jurassic-early cretaceous carbon and oxygen isotope record. J. Geol. Soc. Lond. 161, 695–702. https://doi.org/10.1144/0016-764903-087.

Wendler, I., 2013. A critical evaluation of carbon isotope stratigraphy and biostratigraphic implications for late cretaceous global correlation. Earth Sci. Rev. 126, 116–146. https://doi.org/10.1016/j.earscirev.2013.08.003.